Ocean Engineering 354 (2026) 124883

Contents lists available at ScienceDirect

Ocean Engineering

journal homepage: www.elsevier.com/locate/oceaneng

Research paper

Mitigating underwater noise from offshore wind turbines via individual pitch control

Martín de Frutos [a,*], Laura Botero-Bolívar [b], Esteban Ferrer [a,c]

[a] ETSIAE-UPM - School of Aeronautics, Universidad Politécnica de Madrid, Plaza Cardenal Cisneros 3, Madrid, E-28040, Spain
[b] Mechanical Engineering department, Universidad Industrial de Santander, Carrera 27 Calle 9, Bucaramanga, Bucaramanga, 680001, Colombia
[c] Center for Computational Simulation, Universidad Politécnica de Madrid, Campus de Boadilla del Monte, Madrid, E-28660, Spain

ARTICLE INFO

Keywords:
Individual pitch control
Offshore wind turbine
Noise prediction
Acoustics
Marine mammals

ABSTRACT

This paper proposes a pitch control strategy to mitigate the underwater acoustic footprint of offshore wind turbines, a measure that will soon become necessary to minimize impacts on marine life, which rely on sound for communication, navigation, and survival.

First, we quantify the underwater acoustic signature of blade-generated aerodynamic noise from three reference offshore wind turbines–the NREL 5 MW, DTU 10 MW, and IEA 22 MW using coupling blade element momentum and coupled air–water acoustic propagation modeling. Second, we propose and implement an open-loop individual pitch control (IPC) strategy that modulates the pitch of the blade at the blade passing frequency to attenuate the overall sound pressure level (OSPL) and the amplitude modulation (AM) of the transmitted underwater noise. Third, we benchmark IPC performance against conventional pitch schemes. The results indicate that up to 3 dB reductions in OSPL and a decrease in AM depth of 20% can be achieved with a pitch variation $\Delta\theta \approx 3°$, with limited losses (3-5%) in energy capture. Additionally, we show that the pitch-based noise mitigation strategy predominantly benefits low- and mid-frequency ranges, with limited effectiveness for high-frequency–hearing species. These findings highlight a previously underappreciated noise pathway and demonstrate that targeted blade-pitch modulation can mitigate offshore wind turbine underwater noise impact.

1. Introduction

Offshore wind energy is rapidly expanding as a cornerstone of the global transition to low-carbon power, with installed capacity projected to exceed 250 GW by 2040 (European Commission, 2023). Although the underwater soundscape of offshore wind farms has traditionally focused on the noise of the foundation installation and the emissions of mechanical machinery (Tougaard et al., 2020), an important and underappreciated path remains: the penetration of aerodynamic blade noise from the air into the marine environment. Wind turbine operational noise persists throughout the life cycle of the wind farm (20 to 30 years); therefore, marine life is exposed over the long term, potentially causing changes in behavior (e.g., communication and mating). Aerodynamic noise, generated by blade–airflow interactions, has been extensively characterized in terms of its far-field aerial propagation. However, when these sound waves impinge on the sea surface, a fraction of their energy can be transmitted underwater (Chapman and Ward, 1990). This anthropogenic underwater noise has the potential to cause a masking problem, interfering with the communication, navigation, and foraging behaviors of marine fauna (Erbe et al., 2016).

Regarding wind turbine noise mitigation techniques, most of them are implemented in the design stage (Deshmukh et al., 2019). However, little research is devoted to wind control strategies designed to account for noise emissions. These silent control strategies could be applied to existing facilities. In our previous work, Frutos et al. (2025) we introduced reinforcement learning-based wind turbine control to balance power output and noise reduction in onshore environments. In this work, we will leverage individual pitch control (IPC) to specifically reduce the aerodynamic wind turbine noise that will penetrate the air-water interface.

Individual pitch control came about as a method that focuses mainly on reducing blade loads (Bossanyi, 2003). However, with time, different IPC strategies have been designed for different applications (Jiang et al., 2016). For example, reducing power fluctuations due to tower shadowing (Zhang et al., 2012) or wake manipulation as the recent Helix approaches (Frederik et al., 2020; Taschner et al., 2023; Mohammadi et al., 2025). Regarding noise emissions, Mackowski and Carolus (2021) proposed an IPC scheme to reduce the depth of characteristic modulation of amplitude of near-field wind turbine noise. From a control perspective, load reduction strategies generally implement closed-

* Corresponding author.
E-mail addresses: m.defrutos@upm.es (M. de Frutos), laura.botero@uis.edu.co (L. Botero-Bolívar), esteban.ferrer@upm.es (E. Ferrer).

https://doi.org/10.1016/j.oceaneng.2026.124883
Received 24 October 2025; Received in revised form 13 February 2026; Accepted 27 February 2026
Available online 9 March 2026

loop conventional control methods for IPC, although recent reinforcement learning approaches have been proposed, Coquelet et al. (2022). However, other approaches, such as Helix control, tend to design open-loop analytical IPC schemes. However, to date, no IPC strategy has been explicitly designed to mitigate aerodynamic noise transmitted into the underwater environment, nor to exploit the physical mechanisms governing air–water acoustic transmission.

To the best of our knowledge, this study is the first to propose and systematically evaluate a wind turbine control strategy specifically tailored to reduce underwater acoustic radiation originating from aerodynamic blade noise. The proposed open-loop IPC scheme introduces blade-passing-frequency pitch actuation designed to attenuate the portion of the acoustic field that effectively penetrates the air–water interface, thereby explicitly linking aerodynamic noise directivity, acoustic transmission physics, and control design. In this work, we quantify the underwater acoustic footprint attributable to aerodynamic blade sources of large offshore horizontal-axis wind turbines and evaluate the proposed IPC approach in three reference turbines of increasing capacity: the NREL 5 MW, DTU 10 MW, and IEA 22 MW. To show the validity and generalization for turbines of increasing size, different metrics are addressed: power generation, overall sound pressure level (OSPL) and normal amplitude modulation (AM) depth. Amplitude modulation is recognized as a significant contributor to noise annoyance in humans (Lee et al., 2011). Furthermore, this study provides the first analysis of the impact of different wind turbine control strategies on marine mammal acoustic exposure, thereby bridging wind turbine control design and ecological acoustic assessment within a unified framework.

The paper is organized as follows. In Section 2 a metric is defined to quantify the underwater acoustic footprint and the IPC scheme. Then, in Section 3, this IPC is validated for the three different wind turbines, considering its effect on different species of marine mammals. Finally, in Section 4 we come to conclusions and perspectives.

2. Methodology

An IPC control strategy to reduce the underwater acoustic footprint of wind turbines with minimal impact on power performance is presented in this section. First, how the wind turbine is modeled in both power and noise prediction is described in Section 2.1. Next, in Section 2.2 a metric is designed to assess the underwater acoustic footprint. Finally, the motivation for employing IPC is discussed in Section 2.3, and the IPC scheme is detailed in Section 2.4.

2.1. Wind Turbine Modeling

To compute the power output and noise generation of the wind turbine, OpenFAST (Laboratory, 2024) is used. OpenFAST is an open source wind turbine simulation tool based on blade element momentum theory with coupled multi-physics modules, including aeroacoustics, Bortolotti et al. (2020). The aeroacoustic model employed is the semi-empirical Brook Pope and Marcolini model (Brooks et al., 1989), BPM. There are several studies in the literature that validate the BPM methodology with experimental wind turbine noise measurements, for example, Leloudas et al. (2007), Zhu et al. (2005) or Dorrego et al. (2021) among others.

The two more significant noise sources modeled by the BPM model are the trailing edge (TE) noise mechanism and the leading edge (LE) inflow turbulence noise. TE noise is widely recognized as the dominant aerodynamic noise source in wind turbines, Oerlemans (2011). Moreover, in offshore environments, characterized by low turbulence intensities (5% to 10%), LE noise will be typically low and TE noise dominates. LE noise scales with atmospheric turbulence and rotor speed and cannot be controlled with our pitch-based controller (since our controller does not modify the rotational speed). In contrast, TE noise depends on the parameters of the boundary layer of the blade section, which makes it sensitive to operational conditions, such as the angle of the blade pitch, and shows a low dependency on atmospheric turbulence. In summary, offshore sites exhibit lower turbulence than onshore sites, making TE noise the dominant contribution. Therefore, in this work we only consider the TE noise mechanism in our proposed IPC strategy. The wind turbine controller is implemented from the DRC reference open source baseline controller (Mulders and Van Wingerden, 2018). It has been modified to include an IPC controller that follows the pitch law explained in Section 2.4.

2.2. Wind turbine noise radiated underwater

In this section, we aim to establish a quantitative metric that characterizes the extent to which wind turbine noise can propagate into the underwater environment. Plane wave theory is used to estimate the air-water propagation of acoustic waves. Given the significant contrast in sound speed between air (c_a) and water (c_w), characterized by a speed ratio of $n = \frac{c_w}{c_a} \approx 4.37$, the transmission of airborne noise into water is constrained by Snell's law, given by:

$$c_w \sin\phi = c_a \sin\alpha, \tag{1}$$

where α and ϕ are the incident and refracted angles, respectively.

Snell Cone

Snell law explains how the acoustic waves are refracted when surpassing the air-water interface. Considering a plane interface and the air-water index of refraction n, only the acoustic energy radiated within a conical region, defined by a semi-angle of $\phi_{\text{lim}} = \arcsin(n^{-1}) \approx 13°$, is effectively transmitted to water (Chapman and Ward, 1990), and we denote that region as the "Snell Cone".

Regarding wind turbine noise, most of the sound is generated at the tip of the blade (Oerlemans et al., 2007). Therefore, we consider one Snell Cone per blade located at 95% of the blade length. Each blade's noise is propagated underwater only through its respective Snell Cone. Fig. 1a illustrates the Snell Cone generated by one wind turbine blade.

Additionally, as a consequence of Snell's law refraction, the sound rays that are closer to the limit angle reach much farther in the ocean. In other words, underwater observers far away from the noise source are reached by almost the limit-angle sound rays. Fig. 1b shows how the angle of incidence ϕ approaches the limit angle ϕ_{lim} as the observer is further away from the noise source. Due to strong refraction at the air–water interface, distant observers primarily receive sound rays near the limiting angle. This property will later be used to estimate the overall underwater sound pressure level.

Overall sound power level that penetrates the interface

To quantify the propagation of underwater noise, we consider how much noise irradiated by the wind turbine can exceed the interface. We can then compute the Overall Sound Power Level, OSWL, of the WT taking into account this Snell-cone propagation. We define the OSWL irradiated from the wind turbine that penetrates the air-water interface as follows:

$$\text{OSWL}(t) = 10\log_{10}\left(\frac{1}{p_{\text{ref}}^2}\int_S \sum_{b=1}^{B} S_{pp}^b(\bar{x},t)\chi^b(\bar{x},t)dS\right), \tag{2}$$

where S denotes the area of the air-water interface, $S_{pp}^b(\bar{x},t)$ is the total noise produced by the blade b at the observer location $\bar{x}$ and at instant t, calculated in Pa^2 and integrated over all frequencies. The reference pressure used is $p_{\text{ref}} = 20\mu\text{Pa}$. The function $\chi^b(\bar{x},t)$ acts as a mask for the Snell Cone of each blade, whose area is $\mathcal{A}_{\text{SC}}^b(t)$. So, at each instant and for each observer, we only consider the noise generated by the blades whose Snell cone contains the observer. This masking function is defined as follows.

$$\chi^b(\bar{x},t) = \begin{cases} 1, & \bar{x} \in \mathcal{A}_{\text{SC}}^b(t) \\ 0, & \bar{x} \notin \mathcal{A}_{\text{SC}}^b(t). \end{cases} \tag{3}$$

In practice, we use a BPM method to predict wind turbine noise. This semi-empirical methods require to be evaluated at some specific

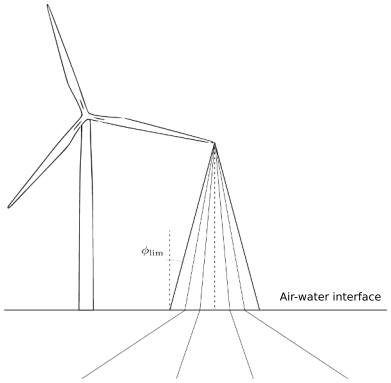

(a) Wind turbine and Snell Cone illustration for one blade. The limit angle ϕ_{lim} and some sound rays following Snell's law are shown.

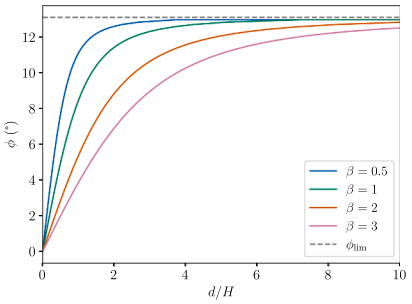

(b) Snell incidence angle with distance d for different depths. The sound source is located at H meters above the air-water interface and the observer is located βH meters deep.

Fig. 1. Illustration of air–water sound refraction effects. On the left, refraction of acoustic rays from a blade-tip noise source governed by Snell's law. On the right, the effect of distance on the Snell incidence angle ϕ.

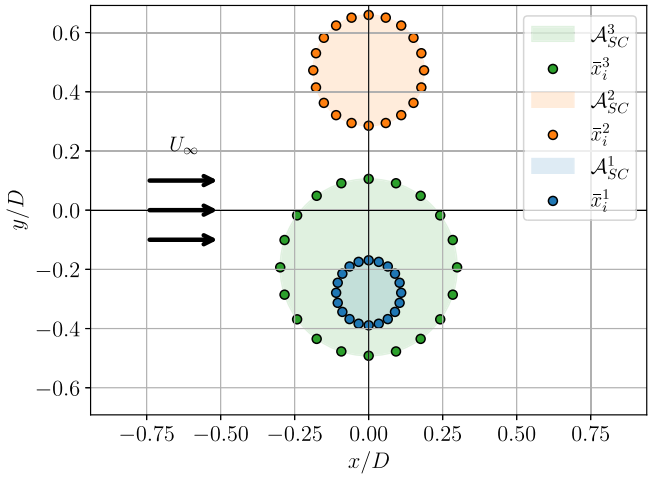

Fig. 2. Observers configuration employed to estimate $\overline{\text{OSPL}}$ at certain time instant for each wind turbine blade. $N_c = 20$ observation points are uniformly distributed along the Snell Cone border. The wind direction is from $-x$ to $+x$, as indicated, and the vertical axis corresponds to z. The view is from above the rotor plane.

observer locations. Therefore, we need to discretize Eq. (2). At each instant of time, we compute the noise of the wind turbine in the observers N_c at the intersection between each Snell Cone blade and the air-water interface; those coordinates are denominated as $\bar{x}^b_i(t)$, with i from 1 to N_c. We only consider observers located at the limiting angle, near the intersection of the Snell cone with the sea surface, since these positions are the most relevant for far-field underwater acoustics (see Fig. 1b). Fig. 2 illustrates the observers used to estimate the overall sound power level integral. From the noise at the selected observer locations, we can compute $\overline{\text{OSPL}}(t)$, defined as the overall sound pressure level averaged on the blade's Snell Cone regions at each time instant,

$$\overline{\text{OSPL}}(t) \approx 10\log_{10}\left(\frac{1}{p^2_{\text{ref}}}\sum_{b=1}^{B}\left(\frac{1}{N_c}\sum_{i=1}^{N_c} S^b_{pp}(\bar{x}^b_i(t),t)\right)\frac{\mathcal{A}^b_{\text{SC}}(t)}{\mathcal{A}_{\text{SC}}(t)}\right), \tag{4}$$

where $\mathcal{A}_{\text{SC}}(t)$ is the sum of the three areas of the Snell cone. The $\mathcal{A}^b_{\text{SC}}(t)/\mathcal{A}_{\text{SC}}(t)$ ratio serves to weight each blade contribution, as the number of observers is the same regardless of the Snell Cone area.

Notice that $\overline{\text{OSPL}}$ represents the overall pressure level that would be heard on average in the Snell cone region of the three blades. However, this sound pressure level is above the interface. We consider the region where the noise will propagate, but we do not employ any transmission loss modeling.

To later estimate the actual sound pressure level at an underwater receiver, the present framework would need to be coupled with an acoustic propagation model. A general formulation for such an estimate is obtained using the point source approximation by Salomons (2001),

$$\text{SPL}(f) = \widehat{\text{SPL}}(f) + \Delta L(f) - \alpha_w(f)d, \tag{5}$$

where $\text{SPL}(f)$, is the sound pressure level spectrum at a certain underwater receiver, $\widehat{\text{SPL}}(f)$ is the sound pressure level spectrum averaged on the Snell Cone and over a rotation and ΔL considers the transmission loss associated with the air-water interface and the underwater reflections. Finally, $\alpha_w(f)d$ accounts for frequency-dependent acoustic attenuation in water, for a receiver at distance d.

Although not directly modeling underwater propagation, $\overline{\text{OSPL}}$ captures the phenomena that will be used in the proposed IPC strategy, that is, the near-field directivity of wind turbine noise and the influence of blade pitch on the generation of aerodynamic noise. Furthermore, the transmission loss ΔL does not depend on the acoustic source. Hence, the noise reduction at an observer due to our proposed IPC scheme is not influenced by the transmission modeling. Thus, $\overline{\text{OSPL}}$ is a suitable metric to validate the efficacy of IPC.

2.3. Why Individual Pitch Control?

There are two different effects that can be leveraged by using IPC to reduce underwater noise propagation. First, due to the characteristics of air-water acoustic transmission, underwater noise perception is primarily influenced by the near-field region, as wind turbine blade noise propagates only within its respective Snell Cone, located beneath the turbine. In this region, the noise fluctuations are higher due to the directivity of the source, as illustrated in Fig. 3a. There, the noise generation is dominated by the blade in the downward position, as reported by Oerlemans et al. (2007). Second, the blade pitch angle is known to significantly affect both aerodynamic power output and noise generation. Generally, increasing the pitch angle leads to a lower angle of attack, and therefore, to decreased power. Consequently, the noise levels of the wind turbine are also reduced with increasing values of pitch angle, see (Maizi et al., 2017; Frutos et al., 2025). However, in the near-field region, these noise oscillations can overlap for different pitch angle values, as shown in Fig. 3b. Based on this observation, a potential strategy is to design an IPC scheme that increases the pitch angle exclusively for the downward-moving blade. This approach would reduce the overall noise by aligning it more closely with low-noise pitch settings, while maintaining high power output, as only one blade is modified at a time.

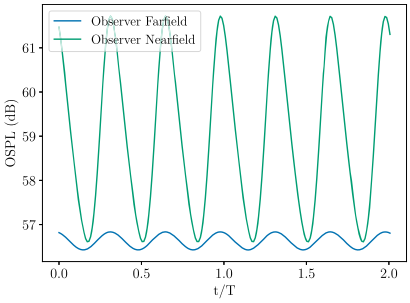

(a) OSPL directivity effect for near-field and far-field observers. The observers are located 50 m downstream and 200 m downstream respectively.

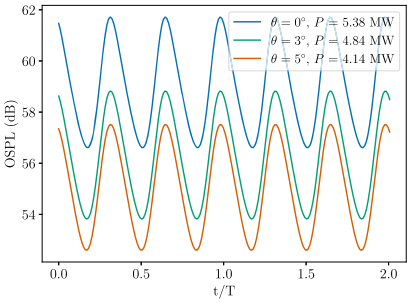

(b) Power, P and noise sensitivity with pitch blade angle, θ for an observer in the near-field, 50 m downstream of the wind turbine.

Fig. 3. Wind turbine noise behavior for different observer positions and blade pitch angle values over two rotor revolutions. Results presented for the NREL 5 MW wind turbine.

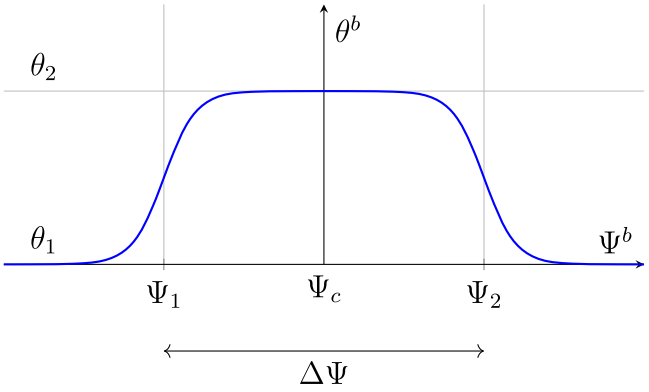

Fig. 4. Pitch law for each blade depending on its phase.

2.4. Pitch Law

We propose an IPC scheme that pitches the blade in the downward position. An analytical law is proposed to ensure smooth pitch variation, which defines each blade pitch angle θ^b depending on the local blade azimuth angle Ψ^b.

$$\theta^b(\Psi^b) = \begin{cases} \theta_1 + \frac{1}{2}(\theta_2 - \theta_1)(1 + \tanh((\Psi^b - \Psi_1)k)), & \text{if } \Psi^b \le \Psi_c \\ \theta_2 + \frac{1}{2}(\theta_1 - \theta_2)(1 + \tanh((\Psi^b - \Psi_2)k)), & \text{if } \Psi^b > \Psi_c. \end{cases} \tag{6}$$

This law sets a high-noise/power pitch value θ_1 and alternates to a low noise-power pitch value θ_2 between the local azimuth positions Ψ_1 and Ψ_2. We define the central phase azimuth position $\Psi_c = \frac{1}{2}(\Psi_2 + \Psi_1)$ and the phase width $\Delta\Psi = \Psi_2 - \Psi_1$. The transition between the values is made using a hyperbolic tangent function with parameter k. The local origin of the azimuth position $\Psi^b = 0$ is when the blade b is vertically facing upward. Fig. 4 illustrates this analytical pitch law.

The parameters of Eq. (6) determine the power-noise trade-off of the IPC scheme. We can give some bounds to k and $\Delta\Psi$ to ensure that the pitch law is applicable to existing offshore wind turbines that can effectively alternate between pitch values.

Usually, wind turbine manufacturers set a maximum pitch rate. For example, in the NREL 5 MW turbine (Jonkman, 2009), the maximum pitch rate allowed in the control is 10°/s. This constraint can be used to bound the maximum steepness of the hyperbolic tangent. Hence, a maximum value for k can be obtained,

$$\max \frac{d\theta^b}{dt} = \Omega \left.\frac{d\theta^b}{d\Psi}\right|_{\Psi_1} = \Omega k \Delta\theta \le \dot{\theta}_{\max} \Rightarrow k_{\max} = \frac{\dot{\theta}_{\max}}{\Omega\Delta\theta}, \tag{7}$$

where $\Delta\theta = \theta_2 - \theta_1$ is the pitch jump and Ω is the speed of the wind turbine rotor. Similarly, we can obtain the minimum phase width required to ensure that the pitch reaches θ_2. Since the transition is a hyperbolic tangent, the final pitch value is reached only asymptotically. We can define the minimum phase to reach at least 95% of θ_2,

$$\tanh\left(\frac{\Delta\Psi k}{2}\right) \approx 1 \Rightarrow \Delta\Psi_{\min} = \frac{2\Omega\Delta\theta}{\dot{\theta}_{\max}} \operatorname{atanh}(0.95). \tag{8}$$

Selecting appropriately the values of the phase width and the pitch jump will define the power-noise trade-off of the IPC scheme. Both $\Delta\Psi$ and $\Delta\theta$ reduce the power extraction and noise generation. Actually, the power generation as a function of these parameters can be estimated as follows

$$P(\Delta\Psi, \Delta\theta) \approx P_{\text{coll}}(\theta_1)\left(1 - \frac{\Delta\Psi}{2\pi}\Delta P(\Delta\theta)\right), \tag{9}$$

where $P_{\text{coll}}(\theta)$ denotes the power generation for a collective pitch θ and $\Delta P(\Delta\theta) = |P_{\text{coll}}(\theta_1) - P_{\text{coll}}(\theta_2)|$ the power difference between collective pitch values.

Fig. 5 illustrates a sensitivity analysis of these parameters for the NREL 5 MW wind turbine. It can be seen how in Fig. 5a the approximate expression by Eq. (9) is recovered. Both phase width and pitch jump reduce power and noise monotonously.

From a manufacturer point of view, these curves could be used to determine $\Delta\Psi$ and $\Delta\theta$ that get certain power losses or minimize specific power-noise metrics. For example, if one needs to comply with noise regulations to reduce 2 dB, one first chooses $\Delta\theta$ and $\Delta\Psi$ that provides the desired noise reduction in Fig. 5b, in our example 3° and 160°, respectively. Then, one could find the power loss that the IPC scheme produces looking at Fig. 5a, in this case approximately $1 - 5.15/5.38 \approx 4\%$.

3. Results and discussion

The IPC scheme proposed in Section 2.4 is evaluated for three offshore wind turbines: the NREL 5 MW (Jonkman, 2009), the DTU 10 MW (Bak et al., 2013), and the IEA 22 MW (Zahle et al., 2024). These wind turbines span a wide range of geometric operational conditions; see Table 1. All results presented are obtained using nominal wind speed and rotational speed conditions.

In Section 3.1, the power-noise trade-off for these three offshore wind turbines is discussed. Two different IPC schemes are proposed and tested. Finally, in Section 3.2, we quantify the effectiveness of the IPC strategy in different groups of marine animals.

As an extension of this work, two appendices are included. In Appendix A we explore how to combine our proposed IPC strategy with closed-loop controllers and a small wind farm test case is evaluated. Finally, in Appendix B we perform a preliminary analysis of the fatigue damage that is produced by this control.

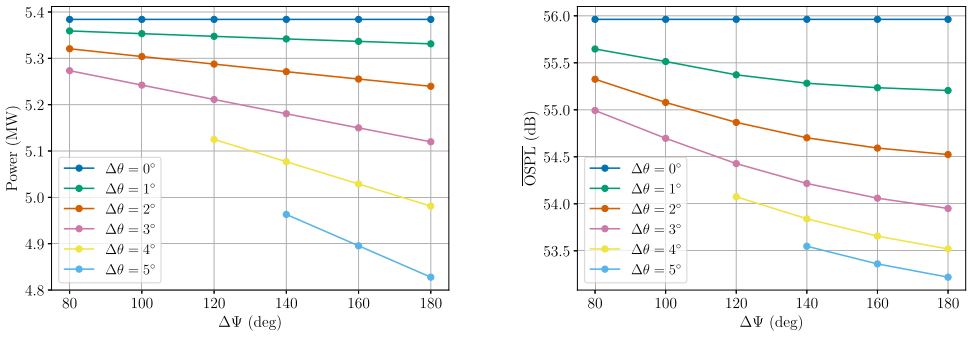

(a) Power generation.

(b) Average noise radiated underwater.

Fig. 5. Sensitivity analysis for the pitch law parameters $\Delta\Psi$ and $\Delta\theta$. Simulations computed for the NREL 5 MW wind turbine.

Table 1
Geometrical and operational (rated) conditions of three large offshore wind turbines.

Characteristic	NREL 5 MW	DTU 10 MW	IEA 22 MW
Hub height [m]	90.0	119.0	170.0
Rotor diameter [m]	126.0	178.4	284.0
Nominal wind velocity [m/s]	11.4	11.4	11.13
Rotor angular velocity [rpm]	12.1	9.6	7.1
Blade tip velocity [m/s]	79.0	90.0	102.0
Blade Pitch [deg.]	0.0	0.0	4.12

3.1. Power and noise balance for three offshore wind turbines

The trade-off between power extraction and wind turbine noise is primarily governed by the pitch angles defined by the pitch control law (see Eq. (6)), specifically θ_1 and θ_2. The selection of these values reflects the relative importance assigned to power generation versus noise reduction.

The high-noise/power angle θ_1 corresponds to the nominal setting of the pitch angle. This is typically optimized for maximum power output. From a control perspective, θ_1 would be the collective pitch angle imposed by a conventional variable-speed controller. In contrast, θ_2 serves as a tunable parameter to balance the power-noise trade-off. Increasing the pitch angle beyond nominal conditions generally results in a simultaneous reduction in both power and noise levels.

This section presents a brief discussion on the impact of pitch jump $\Delta\theta = \theta_2 - \theta_1$ on power generation and noise emissions. Two different IPC schemes are studied, with pitch jumps of $\Delta\theta^1 = 3°$ and $\Delta\theta^2 = 5°$. A higher value of the pitch jump requires a larger phase width, so the pitch has enough time to transition. Hence, different phase widths are used, $\Delta\Psi^1 = 120°$ and $\Delta\Psi^2 = 150°$. Notice that both are larger than $\Delta\Psi_{\min}$ defined by Eq. (8) for each case. The value of both pitch laws k is set as the maximum allowed pitch rate; see Eq. (7). The central phase selected for both strategies is $\Psi_c = 135°$, which corresponds to the middle azimuth position in the downward quarter.

For illustration, in Fig. 6 we present the average overall sound pressure level on the Snell Cone ($\overline{\text{OSPL}}$) produced by each IPC strategy applied to the DTU 10 MW wind turbine. The results corresponding to constant pitch values–namely the nominal angle and increments of +3° and +5°–are also included. Fig. 6a illustrates how the pitch law transitions from following the low noise $\overline{\text{OSPL}}$ curve when the blade is oriented downward to aligning with the high noise curve when the blade noise radiated in the Snell Cone region is minimal. This showcases the pitch law's ability to reduce noise by targeting the most acoustically sensitive positions. Finally, the result $\overline{\text{OSPL}}$ for the entire wind turbine is shown in Fig. 6b. There are some phenomena to consider when analyzing the noise from the three blades. First, it is important to note that the lowest noise levels observed in the single-blade case (see Fig. 6a) are not fully recovered in the full rotor configuration (see Fig. 6b). This is due to the $2\pi/3$ phase difference between blades, when one blade is in a low-noise position, the other two occupy different angular positions. As a result, total wind turbine noise exhibits an overlap of high- and low-noise regions, leading to a reduction in the depth of modulation of the amplitude of the signal, $\overline{\text{OSPL}}(t)$. Another important remark is that the maximum value of $\overline{\text{OSPL}}(t)$ for the entire rotor is lower than the maximum noise level observed for a single blade. This occurs because $\overline{\text{OSPL}}(t)$ represents the average sound pressure level over the Snell Cone region. In the case of three blades, the averaging is performed over the union of the three Snell Cones, which covers a larger area. Since not all blades emit maximum noise simultaneously, spatial averaging across this extended region results in a lower overall peak level.

To evaluate the effectiveness of the two IPC schemes, four key performance metrics are compared across the three wind turbines:

1. Power loss with respect to the nominal operating condition.
$$\text{Power Loss} = \frac{\text{Power}}{\text{Power nominal}} \cdot 100\%.$$
2. Noise generation. We denote $\widehat{\overline{\text{OSPL}}}$ to the overall sound pressure level averaged over the Snell Cone area and over one rotation. Notice that it is either integrating all frequencies of $\widehat{\overline{\text{SPL}}}(f)$ or time averaging $\overline{\text{OSPL}}(t)$, both previously introduced.
3. Power Loss Rate (PLR). This is defined as the power loss in % over the overall sound pressure level reduction compared to nominal conditions.
4. Normal amplitude modulation depth (AM) of $\overline{\text{OSPL}}(t)$. Normal AM measures the amplitude of the overall sound pressure level oscillations caused by the directivity of the dominant trailing edge noise source combined with the time-varying position and orientation of the rotating blades. To compute the AM depth, the method proposed by Lee et al. (2011) is followed.

The results are summarized in Table 2. As expected, the low-pitch jump IPC scheme, denoted θ^1_{IPC}, yields the smallest power losses relative to the nominal case. However, this scheme achieves a more modest reduction in $\widehat{\overline{\text{OSPL}}}$ compared to the higher pitch jump variant, θ^2_{IPC}. In particular, both IPC strategies demonstrate the ability to reduce AM with respect to all constant pitch angle configurations.

The choice between θ^1_{IPC} and θ^2_{IPC} ultimately depends on the relative priority given to power production versus noise mitigation. The low pitch jump scheme θ^1_{IPC}, incurs relatively minor power losses–approximately 5% depending on the turbine–while achieving a ~3 dB reduction in $\widehat{\overline{\text{OSPL}}}$. In contrast, the higher pitch jump scheme (θ^2_{IPC}) can reduce noise by up to 5 dB, but at the cost of power losses reaches approximately 10%.

Our proposed IPC scheme produces a power loss of 1-3 %/dB of noise reduction. Meanwhile, collective pitch offsets produce a much higher PLR. van den Berg et al. (2025) conducted a comparison between different Noise-Reduced Operation (NRO) strategies in industry, the study

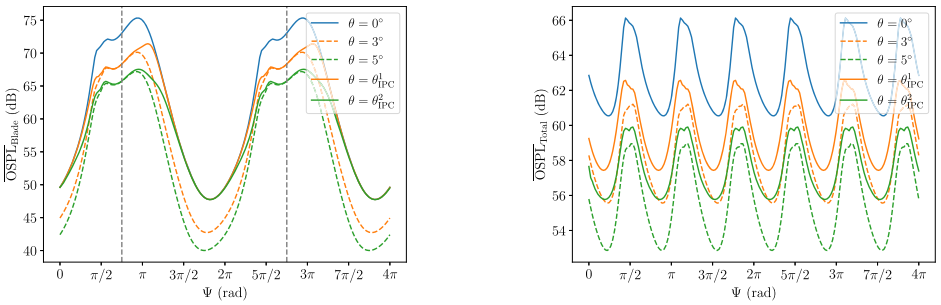

(a) Blade $\overline{\text{OSPL}}$. The dashed lines denotes the central phase Ψ_c of eq. (6) pitch law.

(b) Total $\overline{\text{OSPL}}$. Ψ denotes the azimuth phase of the first blade.

Fig. 6. Comparison of different pitch strategies on the $\overline{\text{OSPL}}$ for the DTU 10 MW wind turbine for two rotor revolutions.

Table 2
Comparison of four performance metrics for different pitch strategies across three offshore wind turbines. The evaluated pitch strategies are: the nominal pitch angle (θ_{nom}), fixed pitch increments of 3° and 5°, and two IPC schemes designed to alternate between the nominal condition and these respective increments.

WT	Metric	θ_{nom}	3°	5°	θ^1_{IPC}	θ^2_{IPC}
NREL	Power loss (%)	0.00	10.16	23.05	3.19	8.45
	$\overline{\text{OSPL}}$ (dB)	55.97	53.68	52.82	54.36	53.45
	PLR(%/dB)	–	4.43	7.33	1.98	3.36
	AM (dB)	7.58	7.79	8.02	7.30	7.22
DTU	Power loss (%)	0.00	4.89	15.39	1.36	5.21
	$\overline{\text{OSPL}}$ (dB)	63.39	58.66	56.25	60.14	57.90
	PLR (%/dB)	–	1.03	2.16	0.42	0.95
	AM (dB)	6.42	6.62	7.10	5.97	5.00
IEA	Power loss (%)	0.00	18.62	36.65	6.17	14.73
	$\overline{\text{OSPL}}$ (dB)	64.34	59.15	56.96	60.81	58.58
	PLR (%/dB)	–	3.59	4.97	1.75	2.56
	AM (dB)	6.80	7.50	7.75	5.90	5.10

stated that the power loss in % per dB was approximately 5%. Therefore, this IPC scheme is more efficient to reduce underwater noise than conventional NRO strategies.

It should be noted that these results were obtained using reference offshore wind turbine models, which are commonly employed in the literature for the evaluation of control strategies. Commercial wind turbines may require retuning of the pitch law parameters to account for differences in turbine geometry and aerodynamic characteristics.

3.2. Influence on marine life

Similarly to humans, marine animals do not hear equally along all frequencies. To characterize how different species of marine mammals perceive sound, Southall et al. (2019) grouped different species into functional hearing groups based on several experimental studies. In this study, we consider the following groups:

- **LF**-cetaceans: Mysticete whales, including minke whale.
- **HF**-cetaceans: Most odontocetes, including the white-beaked dolphin and the pilot whale.
- **VHF**-cetaceans: Narrow-band high-frequency odontocetes, including harbour porpoise
- **PCW**-phocid seals: True seals, including harbor seal and gray seal.

For humans, it is generally agreed that the most reliable way to predict injury risk is to apply a weighting to the SPL spectrum that approximates the inverse of the audiogram, commonly known as A-weighting (dBA). A similar procedure can be performed for the different functional hearing groups of marine mammals (Tougaard, 2021). National Marine Fisheries Service (2016) proposed analytical expressions for these marine weights (or filters) for the different functional groups; see Fig. 7b.

Table 3
$\widehat{\text{OSPL}}$ reduction (dB) using the proposed IPC strategy, θ^2_{IPC}, compared to nominal conditions for the three wind turbines studied and applying different marine animal filters.

WT	Unfiltered	LF	PCW	HF	VHF
NREL	2.58	1.29	-0.46	-0.97	-0.81
DTU	5.35	3.13	0.59	0.09	0.28
IEA	5.60	3.63	0.84	-0.28	-0.29

These group filters are used to assess the reduction in sound pressure level experienced by different groups of marine mammals as a result of the implementation of the IPC scheme. Using the high-pitch jump IPC strategy θ^2_{IPC} the $\frac{1}{3}$-octave $\widehat{\text{SPL}}$ spectrum is shown in Fig. 7a for the DTU 10 MW wind turbine. As observed, the spectrum corresponding to the IPC scheme consistently falls between the spectra obtained with fixed pitch angles, illustrating the intermediate acoustic footprint of the IPC approach.

Table 3 presents the overall reduction in the sound pressure level ΔC due to the IPC scheme relative to the nominal conditions considering different filters for marine mammals. Note that the unfiltered OSPL reduction scales with the size of the wind turbine, which indicates that this IPC control strategy is particularly suitable for large wind turbines, where the wind turbine noise impact is more significant.

As shown in Fig. 7a, the spectral response of $\widehat{\text{SPL}}$ to pitch modifications mainly affects the mid to low frequency range. The IPC-induced noise reduction is concentrated within this frequency band, whereas reductions at higher frequencies are limited, and in some cases, a slight amplification may occur. This results in negative ΔC values (i.e., an increase in SPL) for hearing groups sensitive to high frequencies. The extent of this effect depends on the spectral characteristics of each wind turbine, as illustrated in Table 3. However, note that in the high-frequency range where these species are most sensitive, the baseline wind turbine noise spectrum is already relatively low. Thus, even if the IPC strategy leads to minor increases in SPL at these frequencies, the absolute levels remain low and are unlikely to pose significant acoustic risk.

In general, the IPC strategy proves to be particularly effective for marine species sensitive to mid- and low-frequency noise. In particular, the LF hearing group exhibits the largest reduction, exceeding 3 dB for both the DTU and the IEA wind turbines.

As a final remark, note that the $\widehat{\text{OSPL}}$ reductions due to the control ΔC, are computed above the sea surface. These reductions are still valid at underwater receivers, as all the propagation losses associated with that position do not depend on the control strategy followed; see Eq. (5).

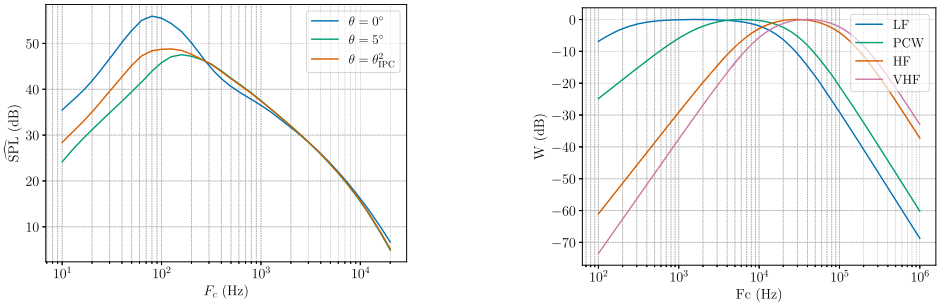

(a) $\frac{1}{3}$-octave $\widehat{\text{SPL}}$ spectrum for the three pitch configurations for the DTU 10 MW wind turbine.

(b) Frequency weighting curves proposed by National Marine Fisheries Service (2016) for different marine animal groups.

Fig. 7. Frequency-domain analysis of wind turbine noise considering IPC and its relevance to marine fauna.

4. Conclusions

In this work, we have quantified how much aerodynamic noise generated by large horizontal-axis offshore wind turbines can penetrate the air–sea interface and contribute measurably to the underwater acoustic environment.

To mitigate this airborne-to-underwater noise, we developed and evaluated an open-loop IPC strategy. By modulating blade pitch at the blade passing frequency, this IPC approach substantially reduces overall sound pressure level and dampens amplitude modulation - a phenomenon known to cause annoyance in humans and likely to affect marine animals similarly. By combining the analyzes of three representative turbines (NREL 5 MW, DTU 10 MW, and IEA 22 MW), we quantified the reductions in sound pressure level due to the proposed IPC method. Furthermore, we computed its effect on marine mammals considering their hearing sensibility.

Our method achieves noise reduction with minimal impact on power performance, confirming a variation in pitch $\Delta\theta \approx 3°$ as an effective compromise between acoustic mitigation and power generation.

Furthermore, our results show that the greatest noise reduction is achieved in the low to mid-frequency range, where the wind turbine noise is most pronounced. They also indicate that pitch control may be ineffective as a mitigation strategy for marine mammals with high frequency hearing. Consequently, the real effect of the IPC strategy will depend on the specific local marine fauna. Therefore, a site-specific ecological assessment should be performed prior to implementing wind turbine noise control measures.

Looking ahead, integrating closed-loop feedback and reinforcement learning algorithms (Frutos et al., 2025; Coquelet et al., 2022) could further optimize pitch schedules in real time, taking into account the changing wind, sea state, and biological risk factors. Preliminary results obtained in Section A suggests that combining the proposed IPC strategy with a variable-speed controller yields to similar noise reductions.

Furthermore, the assumption of a flat sea surface should be revisited, and the propagation model refined to account for the effects of realistic sea surface conditions on acoustic transmission and on the definition of the “Snell Cone”. That being said, the proposed pitch control strategy is designed to reduce the generation of noise by the turbine (and not the propagation); therefore, a reduction in underwater impact should be expected under all sea conditions. Although the effectiveness of the control may vary, we believe that the overall concept remains valid.

By embedding aerodynamic noise considerations in environmental impact assessments and turbine control design, this study paves the way for a more harmonious coexistence between offshore wind development and marine ecosystems.

CRediT authorship contribution statement

Martín de Frutos: Writing – original draft, Visualization, Validation, Software, Methodology, Investigation, Formal analysis, Conceptualization; **Laura Botero-Bolívar:** Writing – review & editing, Validation, Supervision, Methodology, Investigation, Formal analysis, Conceptualization; **Esteban Ferrer:** Writing – review & editing, Validation, Supervision, Resources, Project administration, Methodology, Funding acquisition, Conceptualization.

Declaration of competing interest

The authors declare the following financial interests/personal relationships which may be considered as potential competing interests: Martin de Frutos reports financial support was provided by European Research Council. Esteban Ferrer reports financial support was provided by European Research Council. Laura Botero-Bolivar reports financial support was provided by European Research Council. If there are other authors, they declare that they have no known competing financial interests or personal relationships that could have appeared to influence the work reported in this paper.

Acknowledgement

This research has received funding from the European Union (ERC, Off-coustics, project number 101086075). Also, the authors acknowledge the support of Universidad Industrial de Santander and the Energy and Environment research group (GIEMA). Views and opinions expressed are, however, those of the authors only and do not necessarily reflect those of the European Union or the European Research Council. Neither the European Union nor the granting authority can be held responsible for them.

Appendix A. Closed-loop integration and a wind farm application

As an extension of this study, we discuss how the proposed IPC scheme can be integrated with a collective pitch controller, enabling the wind turbine to adapt to dynamic environmental conditions, e.g., wind speed variations or other wind turbine wakes.

For simplicity, we assess the controller performance when implemented on top of a conventional collective pitch controller. The total pitch angle of each wind turbine blade, θ^b, is defined as

$$\theta^b = \theta_{\text{col}}(\Omega) + \theta^b_{\text{IPC}}(\Phi^b), \tag{A.1}$$

where $\theta_{\text{col}}(\Omega)$ is the collective pitch of a classic Region II - Region III wind turbine controller, Burton et al. (2011). This controller aims to maintain the nominal generator speed under above-rated conditions

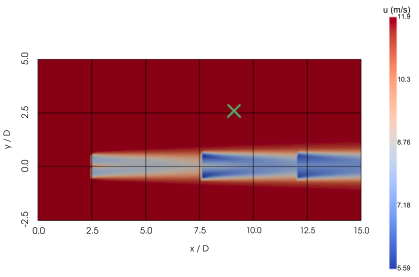

(a) Wind farm layout composed of three NREL 5MW wind turbines. The symbol "×" denotes the location of the underwater observer, which is 60 m deep.

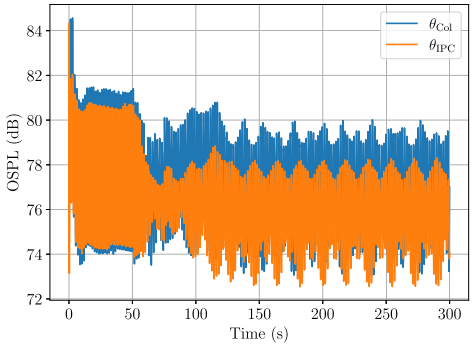

(b) OSPL at the underwater observer "×" using water reference pressure $p_{\text{ref}} = 1\mu\text{Pa}$. Comparison of a standard collective pitch controller against the proposed IPC strategy.

Fig. A.1. Evaluation of the proposed IPC scheme in a small wind farm.

while preserving the optimal collective pitch angle for maximum power capture in below-rated conditions. Meanwhile, the IPC contribution minimizes the underwater noise radiation.

The performance of the combined controller is evaluated on a small wind farm composed of a single row of three NREL 5 MW wind turbines. The wind farm layout used in this simulation is illustrated in Fig. A.1a, together with the corresponding wind velocity field. The simulation is computed using FAST.Farm, an OpenFAST extension for wind farms, Jonkman et al. (2020).

To estimate the overall sound pressure level at the underwater receiver, the transmission loss from the air–water interface to the underwater location is modeled using wave theory (Young, 1973). The air-to-water transmission loss is given by $\Delta L_{\text{a-w}} = 20\log_{10} 2 + 20\log_{10}\left(r_w/r_a\right)$, where the first term accounts for the transmission coefficient at the air–water interface, and the second term represents underwater sound propagation. Here, r_w denotes the distance between the underwater observer and the interface, while r_a represents the distance from the airborne source to the interface, which is approximated by the tower height. The total OSPL at the receiver generated by the wind farm is then estimated as

$$\text{OSPL}(\bar{x}, t) \approx 10\log_{10}\left(\sum_{i=1}^{N} 10^{\left(\overline{\text{OSPL}_i}(t) + 20\log_{10} 2 - 20\log_{10}(r_a^i/r_w^i)\right)/10}\right). \tag{A.2}$$

Fig. A.1b shows the overall sound pressure level estimation at the underwater observer. Note that once the wake is fully developed, the OSPL produced employing the IPC strategy is consistently lower than the one obtained with just a standard collective control. The noise reduction obtained at the farm level is consistent with the single-turbine results reported in Table 2 from Section 3.1, around 2 dB for the NREL 5 MW wind turbine. These preliminary results demonstrate the potential scalability of this IPC strategy to a farm level once coupled with a standard collective pitch controller.

Regarding power generation, Table A.1 reports the power distribution within the wind farm for both control strategies. Since the first turbine operates in the above-rated region, both strategies yield identical power output, since the variable-speed controller employs a PID tracking nominal generator speed. Downstream turbines operate in Region II (underrated conditions). While the second turbine produces slightly less power when using the IPC strategy, it generates a weaker wake, enabling increased power extraction by the third turbine. As a result, the total wind farm power output remains nearly unchanged between the two strategies, with a marginally higher overall power production observed when employing the IPC.

These preliminary results indicate that the proposed IPC strategy may remain effective at the wind farm level. Nevertheless, higher-fidelity modeling approaches are required in future work, as accurate wake characterization and detailed air–water interface modeling are critical for a comprehensive evaluation of the power–noise trade-off.

Table A.1
Power generation of a 3-wind-turbine wind farm under different pitching strategies.

Power (MW)	WT1	WT2	WT3	Farm
θ_{Col}	5.30	3.36	2.10	10.76
θ_{IPC}	5.28	3.23	2.35	10.86

Appendix B. Fatigue analysis of the IPC strategy

Imposing a pitch actuation of the blade-passing frequency increases the mechanical cost of the control. Fatigue loads on wind turbines are commonly measured using the damage equivalent loads metric (DEL).

In the literature, one can find studies that quantify the damage equivalent loads of different IPC strategies. Taschner et al. (2023) quantified the DELs that the Helix control generates for different pitch amplitudes. Following a similar methodology, we include a preliminary DEL analysis to assess the effect of our IPC strategy on the DEL of the wind turbine.

The DEL metric is not directly interpretable in absolute terms and is therefore typically used for comparative purposes across operating scenarios. To provide context for the DEL variations induced by the IPC strategy, two levels of atmospheric turbulence are incorporated in the analysis. By doing so, we can compare if the DEL increase produced by our IPC strategy is comparable to the DEL that the will turbine will encounter naturally, e.g., turbulence effects on the loads.

The study is performed using the DTU 10 MW wind turbine model. Fatigue damage associated with the blade root moments (flap-wise and edge-wise) is evaluated using the DEL formulation proposed by Madsen et al. (1990), which is based on the Wöhler curve. A rainflow counting algorithm is employed to determine the number of load cycles as a function of their respective ranges. The Wöhler exponent is set to 10 for the wind turbine blades. The reference frequency is set to 1 Hz and the simulation time is 10 min. All calculations are performed using the OpenFAST Toolbox, Branlard (2004).

Three IPC configurations are analyzed, corresponding to pitch jumps of $\Delta\theta = 0°, 3°$, and $5°$. Because the flow is turbulent, the IPC strategy is coupled with a standard variable-speed controller. The wind speed remains below-rated; therefore, the controller adjusts only the generator torque to regulate the rotational speed according to wind speed variations. Additionally, three different Turbulence Intensity (TI) values are considered TI = 0%, 1% and 5%. The turbulence is computed using Turb-

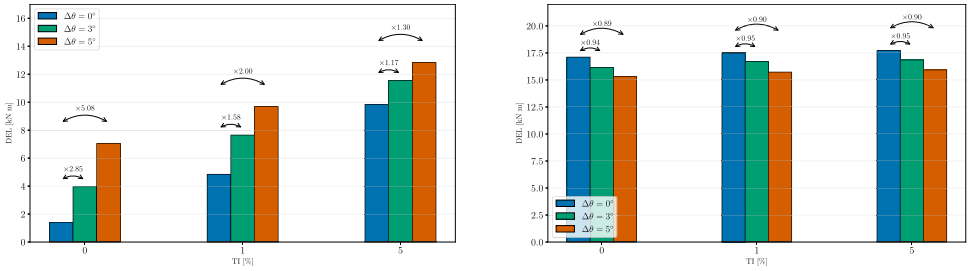

(a) Flap-wise blade root moment. (b) Edge-wise blade root moment.

Fig. B.1. Damage Equivalent Loads (DELs) comparison between a standard variable-speed controller and including our proposed IPC strategy. The DEL are computed for different Turbulence Intensity (TI) inflows.

Sim, a stochastic, full-field, turbulent-wind simulator created by NREL, Jonkman and Kilcher (2012).

Fig. B.1 depicts the influence of TI and our IPC strategy on the DEL for the flap-wise and edge-wise blade root moments. The edge-wise blade root moment is dominated by the gravitational loading (Burton et al., 2011), TI has a minor influence on it and our IPC strategy actually slightly reduces this load, see Fig. B.1b. In contrast, the IPC strategy considerably increases the DEL of the flap-wise blade root moment, as shown in Fig. B.1a. However, this increase is comparable with the one generated by turbulence. Moreover, as turbulence intensity increases, the relative impact of the IPC strategy on the DEL diminishes.

This fatigue assessment indicates that, although the IPC strategy increases the DEL, it is of the same order as that produced by the turbulence that the wind turbine will encounter naturally, and this not significantly increasing fatigue damage. Nevertheless, a more comprehensive evaluation of the mechanical implications of the proposed IPC strategy could be beneficial, prior to real-world implementations.

References

Bak, C., Zahle, F., Bitsche, R., Kim, T., Yde, A., Henriksen, L.C., Hansen, M.H., Blasques, J. P. A.A., Gaunaa, M., Natarajan, A., 2013. The DTU 10-MW reference wind turbine. In: Danish Wind Power Research 2013.

van den Berg, F. G.P., Koppen, E., Boon, J., Ekelschot-Smink, M., 2025. Sound power of onshore wind turbines and its spectral distribution. Sound & Vib. 59 (1), 1716.

Bortolotti, P., Branlard, E., Platt, A., Moriarty, P., Sucameli, C., Bottasso, C.L., 2020. Aeroacoustics Noise Model of OpenFAST. Technical Report. National Renewable Energy Lab.(NREL), Golden, CO (United States).

Bossanyi, E.A., 2003. Individual blade pitch control for load reduction. Wind Energy Int. J. Prog. Appl. Wind Power Convers. Technol. 6 (2), 119–128.

Brooks, T.F., Pope, D.S., Marcolini, M.A., 1989. Airfoil Self-Noise and Prediction. Technical Report.

Burton, T., Jenkins, N., Sharpe, D., Bossanyi, E., 2011. Wind Energy Handbook. John Wiley & Sons.

Chapman, D. M.F., Ward, P.D., 1990. The normal-mode theory of air-to-water sound transmission in the ocean. J. Acoust. Soc. Am. 87, 601–618. https://doi.org/10.1121/1.398929

Coquelet, M., Bricteux, L., Moens, M., Chatelain, P., 2022. A reinforcement-learning approach for individual pitch control. Wind Energy 25 (8), 1343–1362.

Deshmukh, S., Bhattacharya, S., Jain, A., Paul, A.R., 2019. Wind turbine noise and its mitigation techniques: A review. Energy Procedia 160, 633–640.

Dorrego, J.R., Ríos, A., Hernandez-Escobedo, Q., Campos-Amezcua, R., Iracheta, R., Lastres, O., López, P., Verde, A., Hechavarria, L., Perea-Moreno, M.-A., et al., 2021. Theoretical and experimental analysis of aerodynamic noise in small wind turbines. Energies 14 (3), 727.

Erbe, C., Reichmuth, C., Cunningham, K., Lucke, K., Dooling, R., 2016. Communication masking in marine mammals: A review and research strategy. Marine Pollut. Bull. 103 (1-2), 15–38.

European Commission, 2023. Offshore Renewable Energy. Technical Report. European Commission. Accessed: 2025-08-07. https://energy.ec.europa.eu/topics/renewable-energy/offshore-renewable-energy_en.

Frederik, J.A., Doekemeijer, B.M., Mulders, S.P., van Wingerden, J.-W., 2020. The helix approach: using dynamic individual pitch control to enhance wake mixing in wind farms. Wind Energy 23 (8), 1739–1751.

Frutos, M., Marino, O.A., Huergo, D., Ferrer, E., 2025. Enhancing energy generation while mitigating noise emissions in wind turbines through multi-objective optimization: a deep reinforcement learning approach. Wind Energy 28 (8), e70041.

Jiang, Z., Chen, Z., Liu, W., Liu, Y., Wang, X., 2016. A review of individual pitch control for wind turbines. In: 2016 IEEE 11th Conference on Industrial Electronics and Applications (ICIEA). IEEE, pp. 399–404.

Jonkman, B.J., Kilcher, L., 2012. TurbSim User's Guide: Version 1.06.00. Technical Report NREL/TP-5000-46198. National Renewable Energy Laboratory (NREL). Golden, CO. https://www.nrel.gov/docs/fy12osti/46198.pdf.

Jonkman, J.M., 2009. Definition of a 5-MW Reference Wind Turbine for Offshore System Development. National Renewable Energy Laboratory. Golden, CO. NREL/TP-500-38060. 75 pp.

Jonkman, J., Shaler, K., et al., 2020. Fast.farm: A new multiphysics engineering tool for wind-farm-level aero-hydro-servo-elastic simulation. Wind Energy Sci. 5, 721–739. https://doi.org/10.5194/wes-5-721-2020

Laboratory, N. R.E., 2024. OpenFAST. https://github.com/OpenFAST/openfast. Accessed: 2024-04-07.

Lee, S., Kim, K., Choi, W., Lee, S., 2011. Annoyance caused by amplitude modulation of wind turbine noise. Noise Contr. Eng. J. 59 (1), 38–46.

Leloudas, G., Zhu, W.J., Sørensen, J.N., Shen, W.Z., Hjort, S., 2007. Prediction and reduction of noise from a 2.3 MW wind turbine. In: Journal of Physics: Conference Series. 75, IOP Publishing, p. 012083.

Mackowski, L., Carolus, T.H., 2021. Wind turbine trailing edge noise: Mitigation of normal amplitude modulation by individual blade pitch control. J. Sound Vib. 510, 116279.

Madsen, P., Dekker, J., Thor, S., McAnulty, K., Matthies, H., Thresher, R., 1990. Recommended practices for wind turbine testing, 3. fatigue loads. International Energy Agency Programme for Research and Development on Wind Energy Conversion Systems.

Maizi, M., Dizene, R., Mihoubi, M.C., 2017. Reducing noise generated from a wind turbine blade by pitch angle control using CFD and acoustic analogy. J. Appl. Fluid Mech. 10 (4), 1201–1209.

Mohammadi, M.M., Chanprasert, W., Ivanell, S., 2025. Assessment of loads and power generation for a wind farm utilizing helix control strategy. In: Journal of Physics: Conference Series. 3016, IOP Publishing, p. 012022.

Mulders, S.P., Van Wingerden, J.W., 2018. Delft research controller: an open-source and community-driven wind turbine baseline controller. In: Journal of Physics: Conference Series. 1037, IOP Publishing, p. 032009.

National Marine Fisheries Service, 2016. Technical Guidance for Assessing the Effects of Anthropogenic Sound on Marine Mammal Hearing: Underwater Acoustic Thresholds for Onset of Permanent and Temporary Threshold Shifts. National Oceanic and Atmospheric Administration. NOAA Technical Memorandum NMFS-OPR-55. Silver Spring, MD. 178 pp.

Oerlemans, S., 2011. Wind Turbine Noise: Primary Noise Sources. National Aerospace Laboratory (NLR). NLR-TP-2011-011. The Netherlands. 46 pp.

Oerlemans, S., Sijtsma, P., López, B.M., 2007. Location and quantification of noise sources on a wind turbine. J. Sound Vib. 299 (4-5), 869–883.

Salomons, E.M., 2001. Computational Atmospheric Acoustics. Springer Science & Business Media.

Southall, B.L., Finneran, J.J., Reichmuth, C., Nachtigall, P.E., Ketten, D.R., Bowles, A.E., Ellison, W.T., Nowacek, D.P., Tyack, P.L., 2019. Marine mammal noise exposure criteria: updated scientific recommendations for residual hearing effects. Aquat. Mamm. 45 (2), 125–232.

Taschner, E., van Vondelen, A. A.W., Verzijlbergh, R., van Wingerden, J.-W., 2023. On the performance of the helix wind farm control approach in the conventionally neutral atmospheric boundary layer. In: Journal of Physics: Conference Series. 2505, IOP Publishing, p. 012006.

Tougaard, J., 2021. Thresholds for noise induced hearing loss in marine mammals. J. Acoust. Soc. Am. 118, 3154–3163.

Tougaard, J., Hermannsen, L., Madsen, P.T., 2020. How loud is the underwater noise from operating offshore wind turbines? J. Acoust. Soc. Am. 148 (5), 2885–2893.

Young, R.W., 1973. Sound pressure in water from a source in air and vice versa. J. Acoust. Soc. Am. 53 (6), 1708–1716.

Zahle, F., Barlas, T., Lonbaek, K., Bortolotti, P., Zalkind, D., Wang, L., Labuschagne, C., Sethuraman, L., Barter, G., 2024. Definition of the IEA Wind 22-Megawatt Offshore

Reference Wind Turbine. Technical Report. National Renewable Energy Laboratory (NREL), Golden, CO (United States).
Zhang, Y., Hu, W., Chen, Z., Cheng, M., 2012. Individual pitch control for mitigation of power fluctuation of variable speed wind turbines. In: 2012 10th International Power & Energy Conference (IPEC). IEEE, pp. 638–643.
Branlard, E., 2024 OpenFAST Toolbox, https://github.com/OpenFAST/openfast_toolbox
Zhu, W.J., Heilskov, N., Shen, W.Z., Sørensen, J.N., 2005. Modeling of Aerodynamically Generated Noise From Wind Turbines. Journal of Solar Energy Engineering, 127(4), 517–528. https://doi.org/10.1115/1.2035700.